Cellular Automata Modeling of Two Discontinuous Reactions in Fe-13.5 At. Pct Zn Alloy During Ageing and Annealing

JAROSŁAW OPARA, BORIS B. STRAUMAL, and PAWEŁ ZIĘBA

This paper presents a 2D discrete modeling approach for studying two discontinuous reactions, precipitation and dissolution, during the ageing and annealing of a Fe-13.5 at. pct Zn alloy. The cellular automata (CA) method coupled with an analytical solution of the mass transport equations is employed to simulate the behavior of the migrating reaction front and changes in chemical composition within a lamellar modeling system. The developed CA model enables numerical simulation of these phase transformations under conditions defined by experimental data and optimized kinetic parameters. The simulations successfully capture the microstructure evolution, interface migration, solute redistribution, and the *go-and-stop* motion phenomenon during the movement of the reaction front. The results obtained from the CA simulations provide detailed insights into the influence of kinetic parameters on the formation of zinc concentration profiles.

I. INTRODUCTION

DISCONTINUOUS reactions are diffusive phase transformations in the solid-state during which the growth of the resulting phase occurs at a moving reaction front, which is usually a high-angle grain boundary.[1,2] The discontinuous precipitation (DP) reaction occurs during the ageing process when the temperature is reduced to the two-phase region. In Fe Zn alloys, this is a phase transformation during which the supersaturated solid solution α_o decomposes into a lamellar structure consisting of a new phase Γ (rich in solute) and an initial phase α (depleted in solute) with the same crystal structure as the parent phase. The DP reaction follows the scheme: $\alpha_o \rightarrow \alpha + \Gamma$, contrary to the lamellar eutectoid (pearlitic) transformation occurring in steels, where the equation $\gamma \rightarrow \alpha + \beta$ holds true.[3] When the temperature is increased approaching solvus line or above, the reverse transformation begins ($\alpha + \Gamma \rightarrow \alpha_-$), the discontinuous dissolution (DD) reaction. In both DP and DD phase transformations, the reaction front (RF) exhibits a distinct pattern of alternating movement and stopping during its migration. This is the so-called *go-and-stop* motion phenomenon, which is the result of an accumulation of diffusing solute atoms at the RF, whose excessive concentration in the interfacial area causes substantial reduction of the driving force of the phase transformation and consequently stops the migrating reaction front. After the relaxation stage, the boundary diffusion of the solute occurs rapidly, leading to a significant reduction in solute concentration. This reduction creates a sufficiently large driving force for the phase transformation, consequently causing the reaction front to advance.

In the recent years, several papers have been published on the modeling of discontinuous precipitation reaction using two-dimensional discrete models,[4–7] which allow the visualization of the microstructure evolution together with the tracking of the movement of the interface, as well as the graphical representation in maps of the redistribution of solute concentration. The first publications related to discrete modeling of the DP transformation using the phase field (PF) method, were published by Amirouche and Plapp.[4,5] However, the results demonstrated in References 4, 5 are inconsistent with theoretical predictions and experimental observations. Namely, Amirouche and Plapp[4,5] consistently show a disparity in the thickness of solute-rich versus solute-depleted lamellae in their simulations, with the former being significantly thicker. Additionally, the

JAROSŁAW OPARA is with the Łukasiewicz Research Network Upper Silesian Institute of Technology, K. Miarki Str. 12, 44-100, Gliwice, Poland. Contact e-mail: jaroslaw.opara@git.lukasiewicz.gov.pl BORIS B. STRAUMAL is with the Institute of Nanotechnology, Karlsruhe Institute of Technology, Hermann-von-Helmholtz-Platz 1, 76344, Eggenstein-Leopoldshafen, Germany. PAWEŁ ZIĘBA is with the Institute of Metallurgy and Materials Science of Polish Academy of Sciences, Reymonta Str. 25, 30-059, Kraków, Poland.

growth velocities of precipitates reported in their simulations exhibit notable deviations from established theoretical expectations. A more detailed analysis of these inconsistencies can be found in the work of Zięba.[6] More reliable results for PF modeling of discontinuous precipitation on the example of a U-Nb alloy were presented in the work of Duong *et al*.[7] They have shown the importance of the interfacial strain in the phases produced during the DP reaction, and how highly anisotropic boundary diffusion stabilizes the reaction front of DP. In the latest publication of Ladjeroud and Amirouche[8] a three-dimensional (3D) PF model was used to investigate the influence of the additional (third) dimension on the morphology of growing lamellar and fibrous precipitates during DP reaction. Nevertheless, there is a lack of simulation outcomes presenting solute concentration profiles or its distribution that could be referenced to the results of experimental studies. Recently, Opara *et al*.[9] have proposed a discrete DP reaction model that is based on an alternative solution to the PF method, that is the cellular automata (CA) method. Here, contrary to the approach used in PF models,[4,5,7] the modeling of DP reaction is based on experimental data and analytical solution of the diffusion equation. Nevertheless, none of the discrete approaches mentioned here has yet been used for the modeling reverse transformation of the DP reaction, *i.e*., discontinuous dissolution, and even more so for both of these reactions simultaneously. In this work, this challenge will be taken up using the CA method.

The motivation for the application of the CA method is the fact that this approach has been successfully used in modeling diffusion and grain growth at the microscale with the discretization of the interface micro-area at the level of a few nanometers,[10,11] as well as for phase transformations modeling in the solid-state at the mesoscale level.[12–16] Such broad applicability of the CA method is due to the formalism of this method that allows a flexible definition of boundary conditions and transition rules which control the evolution of the system. Additionally, the CA method has gained popularity in the context of microstructure evolution simulation due to several key advantages: its straightforward nature and compatibility with computer architectures, including parallel processing systems, as pointed out by Chopard[17]; its behavior can readily be visualized in graphics, as highlighted by Wolfram[18]; its adaptability allows for the use of diverse state variables and transition rules, as noted by Raabe[19]; its versatility in terms of constitutive elements and local effects, as discussed by Janssens[20]; and its computational efficiency, ability to multi-scale bridging, and physical consistency, as detailed by Liu *et al*.[21] Furthermore, the CA method enables relatively simple integration with other numerical methods, such as the finite difference method[14–16] or the finite volume method,[10,11] as well as the incorporating analytical equations in the computational algorithm to solve mass transport, for example, as shown by Bos *et al*.[12] and recently by Opara *et al*.[9] To cater to readers interested in the CA methodology and its alternatives, such as the Phase Field Method, Monte Carlo method, Vertex models, and others, we recommend the literature references.[19–22] These sources provide comprehensive information on the development and application of cellular automata across various domains of microstructure simulation.

In this study, a discrete model based on the CA method in two dimensions (2D) is developed by coupling with an analytical solution of mass transport equation to investigate the behavior of migrating RF along with changes in chemical composition in the lamellar modeling system during ageing and annealing of a Fe-13.5 at. pct Zn alloy. The distribution of solute concentration in the α phase lamella is then calculated and mapped to the CA calculation space along with the migrating RF to obtain a direct view of the solute segregation and microstructure evolution during discontinuous reactions. This kind of model imminently contains numerous assumptions and simplifications which will be discussed in section with model presentation. After a description of the simulation settings, the capabilities of the CA model will be given for a simulation of DP and DD reactions.

II. MODEL CONCEPT

A. *CA Model for Discontinuous Reactions*

In this work, a 2D CA model is built to simulate the microstructure evolution during discontinuous reactions (DP and DD) at the lamellar level. The assumptions and basis of CA modeling of the discontinuous precipitation (like approximation of RF using the sharp interface concept, unified temperature field, ideal thermal conditions) were presented in detail in the previous work of Opara *et al*.[9] Therefore, a description of the CA method has been shortened. And the focus is put on the key assumptions and modeling aspects that relate to DD reaction. Note, that the aforementioned assumptions applied in DP modeling are also valid in the CA model of DD reaction.

During DD, the backward migration of the reaction front proceeds at the expense of two individual phases, products of the DP reaction, *i.e*., a solute-rich Γ phase lamella and a solute-depleted α phase lamella. In effect, the formation of a dissolved phase $\Gamma_{\sim}$ and an inhomogeneous $\alpha_{\sim}$ solid solution is observed. Therefore, the more appropriate description of the DD reaction seems to be $\alpha + \Gamma \rightarrow \alpha_{\sim} + \Gamma_{\sim}$ instead of previously commonly used $\alpha + \Gamma \rightarrow \alpha_{\sim}$ and it will be used consequently in the present paper. This transformation is manifested by a so-called "ghost images" of the previous positions of the Γ lamellae at which the maximum value of the solute content is expected.[23] The growing phases ($\alpha_{\sim}$ and $\Gamma_{\sim}$) are separated between two parent phases (α and Γ) by the two types of interface $\alpha_{\sim}/\alpha$ and $\Gamma_{\sim}/\Gamma$. Furthermore, these four phases can meet in the so-called quadruple point identified as a $\alpha_{\sim}/\alpha/\Gamma_{\sim}/\Gamma$ interface. Additionally, between alternating lamellae of Γ and α phases, an interface Γ/α is also defined. The definition of interfaces between a combination of the following phases α_{o}, $\alpha_{\sim}$, $\Gamma_{\sim}$ in the CA space is neglected because

they do not play an important role in the calculations. Furthermore, it is hard to identify them definitively on micrographs from transmission (TEM) or scanning (SEM) electron microscope. Figure 1(a) shows a scheme of the cellular automata grid in which all considered phases and types of interfaces are depicted for the simulation of the discontinuous dissolution in the Fe Zn alloy. Meanwhile, Figure 1(b) provides a detailed view of a cellular automaton representing the hypothetical interface and illustrating its growth during the DD reaction. It is important to mention that, in the CA model calculations, each cell is identified by only one phase or interface state.

The CA method definition in the extended version for modeling physical phenomena at the microscale level, regarding the classical one,[17,18] is formulated based on five elements: the CA space (Ω), *i.e.*, a grid of cells that discretizes the modeling area; a finite set of states (Y) to identify individual cells in the computational algorithm; functions with implemented sub-models that calculate local parameters of the physical process, which next are allocated to the suitable state variables of each cell (F); neighborhood (N), composed of a set of all nearest surrounding cells around the central one, which is used in computations of CA rules; the CA transition rules (R) that determine the evolution of the system based on logical operations. The mathematical description of the CA method can be written as follows:

$$\mathrm{CA} = \langle \Omega, Y, F, N, R \rangle \qquad [1]$$

The microstructure evolution can be simulated properly by the proposed CA model when all of its components, like dedicated sub-models of inhomogeneous phase growth and solute boundary diffusion, are correctly defined and transitions rules are synchronously called defining the state of each cell based on the previous states of its neighbors and the cell itself.

B. *Main Assumptions*

The CA model space is a two-dimensional regular square grid with equal spacing (Figure 1(a)), that states the discretization of the modelled microstructure section according to the idea of a digital material representation (DMR). In this concept, CA space represents a volume of real material with its features (*e.g.*, grains, sub grains, grain boundaries) presented explicitly.[24,25] The quantitative description of the microstructure evolution during DD reaction, including the microstructure morphology and solute precipitation, is possible when each CA cell is defined with three state variables:

(1) the phase state variable, which determines whether the cell represents the phases α_o, α, Γ, $\alpha_{\sim}$, $\Gamma_{\sim}$, or the mobile reaction fronts Γ/α_o, α/α_o, $\Gamma/\alpha_o/\alpha$, $\alpha_{\sim}/\alpha$, $\Gamma_{\sim}/\Gamma$, $\alpha_{\sim}/\alpha/\Gamma_{\sim}/\Gamma$, the so-called transition states, and the stationary interface Γ/α;

(2) the solute concentration variable, which determines the average concentration of solute in the cellular automaton;

(3) the phase volume fraction variable of $\alpha_{\sim}$ or $\Gamma_{\sim}$, which quantifies the degree of $\alpha \rightarrow \alpha_{\sim}$ or $\Gamma \rightarrow \Gamma_{\sim}$ transformations in the frontal cells identifying the $\alpha_{\sim}/\alpha$ or $\Gamma_{\sim}/\Gamma$ reaction fronts, respectively;

The state variables' values of each CA cell are updated at each time step according to sub-models and transition rules described in Sections II D and II E.

The computational algorithm with the 2D CA model for the discontinuous dissolution transformation is implemented with the following assumptions:

- In calculating the growth of the new phases, the interface at the quadruple point $\alpha_{\sim}/\alpha/\Gamma_{\sim}/\Gamma$, is treated as the reaction front $\alpha_{\sim}/\alpha$, where the transformation occurs according to the $\alpha \rightarrow \alpha_{\sim}$ scheme.
- The influence of the starting microstructure on phase transformations was taken into account in the CA

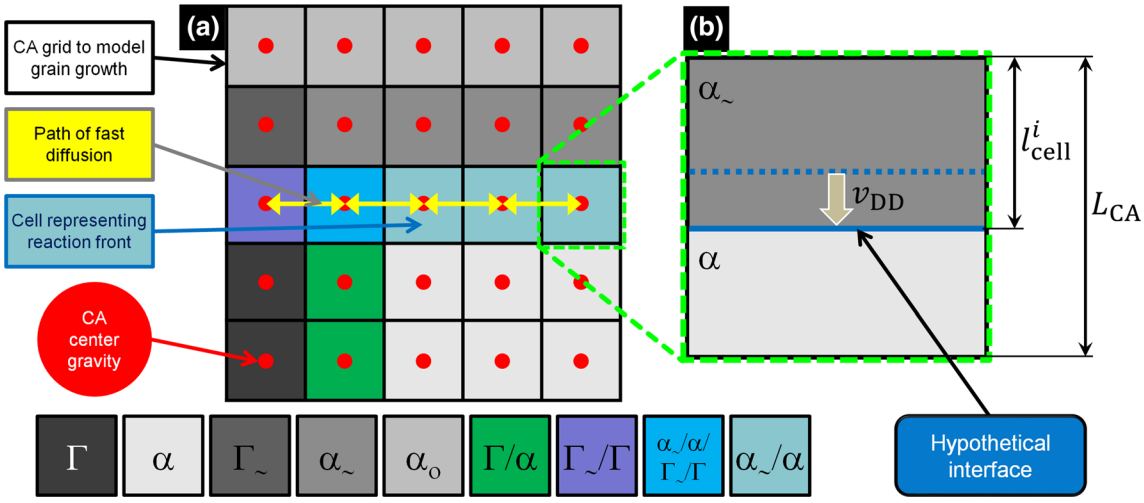

Fig. 1 Grid scheme (*a*) presenting CA space to model inhomogeneous phase growth and solute boundary diffusion during discontinuous dissolution, and a detailed view of a cellular automaton (*b*), illustrating a hypothetical interface and definitions of key parameters: the side width of the CA cell (L_{CA}). (Color version of figure is available online).

model through the use of the digital material representation scheme.

- Only the isotropic growth of the new phase at the steady-state during the DD reaction by giving constant and identical migration rates to both reaction fronts $\Gamma_{\sim}/\Gamma$ and $\alpha_{\sim}/\alpha$, is considered.
- The product of the DD reaction is a two-phase dissolved region, formed at the expense of the lamellar DP structure (consisting of α and Γ lamellae), in which a chemically inhomogeneous $\alpha_{\sim}$ phase and a chemically homogeneous $\Gamma_{\sim}$ phase are included, both retaining the same crystallography as the parent lamellae.
- An analytical equation for modeling the solute diffusion was used in the computational algorithm to determine the Zn concentration profile in the place of the dissolved $\alpha_{\sim}$ phase.
- The Zn concentration in the newly formed $\Gamma_{\sim}$ solid solution takes a constant value according to the assumed concentration just close to the tip of the solute-rich Γ lamella.
- To accurately simulate the *go-and-stop* motion, the CA simulations are based on inputs from tabular data, where details about the reaction front velocity, its movement characteristics, and the kinetic parameter z are specified.
- A von Neumann neighborhood (*i.e.*, four cells adjoining the sides to the central one) is applied in the definition of CA transition rules.

C. *Digital Material Representation*

In order to establish the starting microstructure in the numerical simulations of DP and DD using the CA model, a digital material representation scheme was used according to the approach proposed by Opara and Wrożyna.[26] A digital image of the starting microstructure for numerical simulations can be generated either from a properly prepared structure outline from a metallographic picture or a schematic drawing of the microstructure, as shown in the DMR scheme presented in Figure 2. A detailed description of the procedures used for the conversion of the DP microstructure in the form of raster images into their digital material representation for the CA model can be found in Reference 9.

Figure 2(d) presents the result of digitalization with a zoomed-in section of the DMR that precisely shows the cellular automata discretizing the RF and the grains of the four different phases. Such a discrete modeling approach enables tracking the reaction front's position implicitly (see the hypothetical course of which is outlined in Figure 2(d)), and in consequence, simulating the growth of new phases in a virtual microstructure.

D. *Mathematical Modeling of DP and DD Reactions*

Generally, the theory of discontinuous reactions modeling is founded on the linear relationship between the migration velocity v of the interface, in other words, the growth rate, and the total driving force of the transformation ΔG,[3,27,28] *i.e.*,

$$v \quad M\Delta G \qquad [2]$$

with M as the interface mobility.

Tu and Turnbull[29] applied an analytical approach to model the DD reaction, which is based on diffusion equation proposed by Cahn,[27] in the following form:

$$D_b\delta\frac{\mathrm{d}^2c_b}{\mathrm{d}x^2} \quad v(c_{\sim}(x) \quad c(x)) \quad 0 \qquad [3]$$

where D_b and c_b are the boundary diffusivity and concentration, respectively; δ is an effective thickness of the reaction front assumed to be a planar boundary (see Figure 2(b)); x is the coordinate along the reaction front which is normal to the lamellae; $c(x)$ is the solute concentration profile across the α phase lamellae resulting from the DP process; $c_{\sim}(x)$ is the solute concentration profile left behind the receding RF of the DD reaction.

Zięba and Pawłowski[30] introduced a modification of the Tu-Turnbull theory,[29] consisting of the separation of the kinetic parameters of the DP reaction from those of the DD reaction. Consequently, the determination of the concentration profile of the solute ($c_{\sim}(x)$) in the grain of the $\alpha_{\sim}$ phase, which arises in the x-axis parallel to the moving front of the $\alpha_{\sim}/\alpha$ reaction, is based on the following equation:

$$c_{\sim}(x) \quad c_o + A\sinh(zx\lambda_\alpha) + B\cosh(zx\lambda_\alpha) + \frac{a}{p^2 \quad z^2}\cosh(px\lambda_\alpha) \quad \frac{b}{p^2 \quad z^2}\sinh(px\lambda_\alpha) \qquad [4]$$

where λ_α is the thickness of the α lamella, in other words, interlamellar spacing; p, z, A, B, a and b are the Eq. [4] parameters that enable presenting it in a readable form and can be determined from the following relations:

$$p \quad \left(\frac{v_{\mathrm{DP}}}{s\delta D_b}\right)^{\frac{1}{2}} \qquad [5]$$

$$z \quad \left(\frac{v_{\mathrm{DD}}}{s\delta D_b}\right)^{\frac{1}{2}} \qquad [6]$$

$$A \quad B\tanh\left(\frac{z\lambda_\alpha}{2}\right) \qquad [7]$$

$$B \quad c^* \quad c_o \quad \frac{a}{p^2 \quad z^2} \qquad [8]$$

$$a \quad (c_o \quad c_{\alpha/\Gamma})z^2 \qquad [9]$$

$$b \quad a\tanh\left(\frac{p\lambda_\alpha}{2}\right) \qquad [10]$$

where s is the segregation factor; v_{DP} and v_{DD} are the migration velocities of DP and DD reaction fronts, respectively; c_{o} and c^* are the solute concentrations of the matrix (the initial alloy composition) and the newly

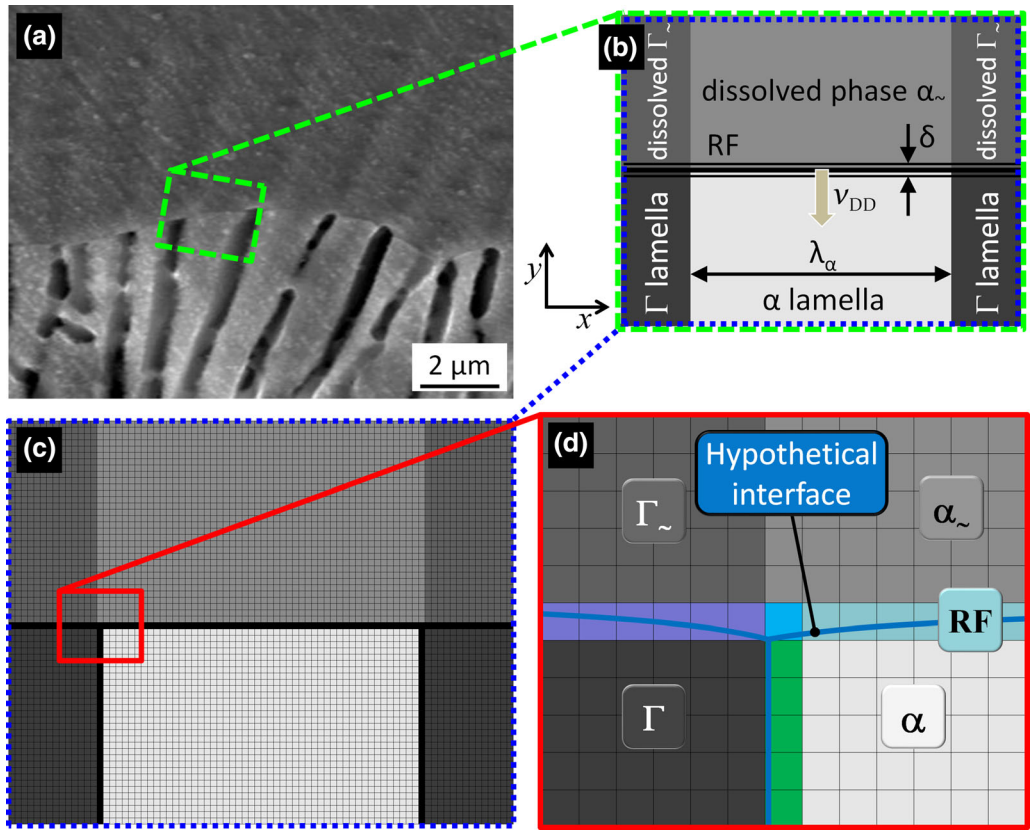

Fig. 2 Scheme showing the concept of digital material representation based on digitalization of the SEM micrograph of Fe-13.5 at. pct Zn alloy aged at 450 K for 2.5 h and subsequently dissolved at 650 K for 2 min (*a*) through the reproduced arrangement of an individual cell when the DP reaction has stopped (*b*) and its conversion into cellular automata grid (*c*). Zoomed fragment of the CA grid (*d*) presents the hypothetical interface (RF) and in effect implicit character of its tracking in the CA model.

formed $\alpha_\sim$ solid solution close to tip of the solute rich Γ lamella, respectively; $c_{\alpha/\Gamma}$ is the solute concentration in the α lamella at the α/Γ interface. It is interesting to note that the parameter p for describing the kinetics of the DP reaction is originally related to Cahn's parameter C[27] by the simple relationship $p \quad \sqrt{C}/\lambda_\alpha$.

In the case of DP reaction modeling, an analytical equation developed by Cahn[27] to determine the solute concentration profile ($c(x)$) in the α lamella that arises in the x-axis, parallel to the moving α/α_o reaction front, is commonly used in the following form:

$$c(x) \quad c_o \quad (c_o \quad c_{\alpha/\Gamma}) \frac{\cosh\left[(x \quad 0.5)\sqrt{C}\right]}{\cosh\left(0.5\sqrt{C}\right)} \qquad [11]$$

In this work we mainly focus on the theoretical description of the DD reaction modeling, therefore for more details about the parameters in Eq. [11], we refer a reader to the articles dedicated to the modeling of DP reaction.[1,9,31]

E. *CA's Governing Equations for DD Reaction*

The growth of inhomogeneous $\alpha_\sim$ solid solution during DD reaction is described in the CA model by the grain growth length parameter (l^i_{cell}), as shown in Figure 1(b). This internal parameter of cellular automata is determined according to an explicit Euler scheme, representing the interface (i), in other words, frontal cells with the reaction front, at each time step (Δt) by integrating after the time (t) the migration velocity of the interface (v), as follows:

$$l^i_{\text{cell}}(t + \Delta t) \quad l^i_{\text{cell}}(t) + v\Delta t \qquad [12]$$

Consequently, only in frontal cells of the CA model a volume fraction of the transformation is calculated, using following formula:

$$F^i_{\text{cell}} \quad \frac{l^i_{\text{cell}}}{L_{\text{CA}}} \qquad [13]$$

where L_{CA} is the side width of CA, also known as the size of the cellular automaton (see Figure 1(b)). On the foundation of the presented Eqs. [4] and [13], the following transition rules were formulated to define CA's set of states during the growth of the newly formed inhomogeneous $\alpha_\sim$ phase and accompanying changes in the solute concentration:

$$Y^i(t + \Delta t) \quad \begin{cases} \alpha_\sim \Leftrightarrow F^i_{\text{cell}} \geq 1 \wedge Y^i(t) & \text{RF} \wedge \alpha \rightarrow \alpha_\sim \\ \Gamma_\sim \Leftrightarrow F^i_{\text{cell}} \geq 1 \wedge Y^i(t) & \text{RF} \wedge \Gamma \rightarrow \Gamma_\sim \\ Y^i(t) \end{cases} \qquad [14]$$

$$c^i(t+\Delta t) = \begin{cases} \text{eq}(4) \Leftrightarrow Y^i(t+\Delta t) = \alpha_\sim \wedge Y^j(t) = \alpha \\ c^* \Leftrightarrow Y^i(t+\Delta t) = \Gamma_\sim \wedge Y^j(t) = \Gamma \\ c^* \Leftrightarrow Y^i(t+\Delta t) = \alpha_\sim/\alpha/\Gamma_\sim/\Gamma \\ c^i(t) \end{cases} \quad j \in N_N(i) \qquad [15]$$

$$Y^j(t+\Delta t) \quad \begin{cases} \text{RF} \Leftrightarrow Y^j(t) \quad \alpha \wedge Y^i(t+\Delta t) \quad \alpha_\sim \\ \text{RF} \Leftrightarrow Y^j(t) \quad \Gamma \wedge Y^i(t+\Delta t) \quad \Gamma_\sim \\ \text{RF} \Leftrightarrow Y^j(t) \quad \Gamma/\alpha \wedge Y^i(t+\Delta t) \quad \alpha_\sim/\alpha/\Gamma_\sim/\Gamma \\ Y^j(t) \end{cases} \quad j \in N_N(i) \qquad [16]$$

where Y^i is the state of cell representing the interface (i) with the migrating RF in which the growth calculations are performed, Y^j is the state of adjacent cellular automata with the frontal one, $N_N(i)$ is the von Neumann neighborhood of the cell representing the interface, and c^i is an internal variable from set of states that identifies the average concentration of a solute in a cell with an interface.

The Eqs. [14] through [16], represent the cellular automata transition rules that are called at each computational step after the change of a discrete segment of time. These CA's rules one can interpret as follows. According to Eq. [14], once the phase volume fraction variable of transformation (F^i_{cell}) exceeds the value of 1 in the frontal cellular automaton representing the RF state, which means that its growth length (l^i_{cell}) has reached the size of the side width of CA (L_{CA}), the cell changes its so-called transition state into the phase state as the newly formed inhomogeneous $\alpha_\sim$ solid solution or dissolved $\Gamma_\sim$ phase respectively to phase transformation occurrence $\alpha \rightarrow \alpha_\sim$ or $\Gamma \rightarrow \Gamma_\sim$. Immediately after that, a new value with the average solute concentration is attributed to the solute concentration variable of the cellular automaton (Eq. [15]), which transformed into the $\alpha_\sim$ or $\Gamma_\sim$ phase. The Zn concentration in cells with the dissolved $\alpha_\sim$ phase is calculated based on Eq. [4], whereas a constant value of c^* is assigned to cells representing the $\Gamma_\sim$ phase or $\alpha_\sim/\alpha/\Gamma_\sim/\Gamma$ interface. Thereafter, in compliance with Eq. [16], cells with the state (Y^j) of the parent phases (Γ and α) or the immobile Γ/α interface that are in the closest vicinity (von Neumann neighborhood) of the cellular automaton with the state (Y^i) of the newly formed phases ($\alpha_\sim$ or $\Gamma_\sim$) or interface ($\alpha_\sim/\alpha/\Gamma_\sim/\Gamma$), are changed into frontal cells (RF). Their growth length (l^i_{cell}) in succeeding steps is determined according to Eq. [12]. When the above conditions described based on Eqs. [14] through [16] are not valid, the considered cellular automaton maintains its previous state.

F. *Numerical Implementation of the Algorithm with the CA Model*

The equations presented in sections above (II D and II E) are solved iteratively at each time step throughout a fixed annealing process simulation time or until DD phase transformation is fully completed. The computational steps are as follows:

(1) Virtual microstructure (digital material representation) initialization at the lamellar level for DD reaction based on results from previous simulations of DP phase transformation and with the defined effective thickness of RF (δ).
(2) Initialization and calculation of the DD reaction characteristic parameters, such as the migration velocities of discontinuous reaction fronts (v_{DP} and v_{DD}), the boundary diffusivity (D_b), and the interfacial solute concentrations ($c_{\alpha/\Gamma}$, c^*) which are generally constant for the considered process of isothermal annealing.
(3) Determination of the time step value (Δt).
(4) Time step increment ($t \quad t + \Delta t$).
(5) Computation of the grain growth length parameter (Eq. [12]) and following volume fraction of the transformation (Eq. [13]) at each cellular automata with the phase state variable representing the RF.
(6) Update of CA's set of states based on Eqs. [14] through [16] and calculation of the solute concentration in the grain of the $\alpha_\sim$ phase according to Eq. [4] in the case where applicable.
(7) Repeat steps 4 6.

Note that the time step definition to provide the numerical calculations stability as well as special procedures for speed-up of computations, inter alia frontal cellular automata (FCA) concept,[32] are accurately described in the related work.[9]

The presented 2D CA model is implemented as a computer program with a graphical user interface using the C++ language with object-oriented programming (OOP) technique. This discrete computational tool is dedicated to performing numerical simulations of the competing new phase growth and solute diffusion during discontinuous reactions.

III. SIMULATION SETTINGS AND INITIAL CONDITIONS

The simulated material is a Fe Zn alloy with 13.5 at. pct concentration of Zn, which was recently investigated in terms of DD and DP reactions.[31,33–35] The steady-state growth of discontinuous reactions DP and DD, was numerically simulated accordingly to conditions presented in Table I.

The simulation's initial conditions were determined using experimental data and numerical tests as outlined in Reference 33. The DP reaction simulation was performed at constant temperature of 723 K (~450 °C) for 1 seconds that correspond to the ageing thermal process conditions. The relatively short time of one second that was chosen to simulate the DP reaction relates to the experimental results, obtained in other works,[31,35] which concern the growth of the α phase lamella, with similar dimensions, at an identical rate of 45 nm/s. The constant growth of discontinuous precipitates, with velocity v_{DP} 45 nm/s, was simulated for

two critical cases with Cahn's parameter, *i.e.*, $C = 1.74$ and $C = 7.23$. Subsequently, the DD reaction simulation was carried out after the fast heating process, neglected in the simulations, to the annealing temperature, equal to 923 K (~650 °C). The isothermal growth of dissolved phases was simulated with a constant velocity equal to v_{DD} 0.5 nm/s for 80 seconds, taking into account the *go-and-stop* motion during movement of the interface. In order to efficiently control the simulation process of RF *go-and-stop* motion, the tabular data with values of the parameter z as a function of time were directly implemented in the code of the computer program with the CA model for the DD reaction. The input data with values of the z parameter for one cycle of *go-and-stop* motion and two extreme C parameters are presented in Table II. The z parameter values were determined using a criterion of the applicability of the Zięba and Pawłowski[30] Eq. [4] as is shown in Reference 23 Figure 60. For this purpose, a dedicated numerical algorithm was implemented as a computer program determining the z parameter value, which used in Eq. [4] allows obtaining the solute concentration profiles satisfying the condition with equality of areas above and under the level of the initial alloy solute concentration (c_o). The procedure to determine the z parameter is clearly presented in Appendix A. The value of the zinc diffusion coefficient in the Fe Zn alloy was calculated based on the equations with a triple product of diffusivity (see Table I). Next, this value was used to determine the time step value according to the numerical calculations stability as was presented in the related work.[9]

Note that the DP reaction's result in the form of digital microstructure representation was an input to the DD reaction simulation. While the initial microstructure used in the simulations of the DP reaction was generated according to the DMR concept on a two-dimensional square grid of cellular automata as is shown in the related work.[9] In the CA space (*i.e.*, computational domain) a set containing the single α phase lamellae with two neighboring Γ phase lamellae and the surrounding α_o parent phase was considered. During DD reaction simulation the dissolved phases ($\Gamma_{\sim}$ and $\alpha_{\sim}$) arise at the expense of the DP reaction products (Γ and α). The movement of the RF during the DP reaction as well as the reverse DD reaction with receding RF into the two-phase structure occurs only in the y-axis according to the Cartesian coordinate system. It is assumed that the starting position of discontinuous precipitate lamellae are found to be at an early stage of the steady-state growth just one second before the beginning of DD reaction. Therefore, their height is small and occupies the size of only one cellular automaton. Based on data presented in Table 4 in Reference 33 the width of the α lamella was fixed as 150 nm and based on the experimental observations the Γ lamella width was assumed to be 10 times smaller.[31] Regarding the assumed RF velocities during DP and DD reactions and resulting movement distances (see Table I), for the convenient and transparent presentation of the results with DMR, the CA grid height was established as half of its width. On this basis and adopting the side width (L_{CA}) of the cellular automaton as 1 nm, the size of the CA space was 180 × 90, *i.e.*, 16,200 cells, which cover the physical region of modeling equal to 180 × 90 nm^2. The reflective boundary conditions at the edges of the CA grid were applied to ensure the stability of the numerical simulations of the discontinuous reactions. This guarantees the avoidance of undesirable modeling effects,

Table I. Simulation Settings

Thermal Process	Ageing	Annealing
Discontinuous Reaction (Phase Transformation)	DP	DD
Isothermal Process Temperature (T_i)	T_i = 723 K (~450 °C)	T_i = 923 K (~650 °C)
Isothermal Process Time (t_i)	t_i = 1 s	t_i = 80 s
Velocity of Reaction Front (v)	v_{DP} = 45 nm/s	v_{DD} = 0.5 nm/s
Movement Distance (MD)	MD = 45 nm	MD = 25 nm
Physical Region of Modeling (CA Grid Size)	180 × 90 nm^2 (180 × 90 cells)	
Thickness of α Lamella (λ_α)	λ_α = 150 nm	
Thickness of Γ Lamella (λ_Γ)	λ_Γ = 15 nm	
Two Critical Values of Cahn's Parameter (C)	C = 1.74 or C = 7.23	
Parameter z for DD Reaction Dedicated to *Go-and-Stop* Period Simulation (Tabular Data from the Defined Range)	—	$z = 1.24 \div 1.77 \times 10^7\ m^{-1}$
Triple Product of Diffusivity ($s\delta D_b$) (Grain Boundary Diffusivity)	$s\delta D_b = \frac{v_{DP}\lambda_\alpha^2}{C}$ m^3/s	$s\delta D_b = \frac{v_{DD}}{z^2}$ m^3/s
Solute Concentration in the α Lamella at the α/Γ interface ($c_{\alpha/\Gamma}$)	$c_{\alpha/\Gamma}$ = 4.11 at. pct Zn	
Solute Concentration in the Γ Lamella (c_Γ)	c_Γ = ~ 69.0 at. pct Zn	—
Solute Concentration in the Newly Formed $\alpha_{\sim}$ Solid Solution at the Tip of the Solute Rich Γ Lamella (c^*)	—	c^* = 16 at. pct Zn
Reference Data Source	[33]	

such as contacting different phases on opposite sides of the CA grid edges.

The initial chemical composition of phases present in the modeling space was assigned according to the following assumptions. In the α_o and Γ phase lamellae the solute concentration (Zn-content) was constant and homogeneous equal to the average zinc concentration (c_o 13.5at. pct Zn) in the investigated Fe Zn alloy and equilibrium concentration (c_Γ $\sim$ 69at. pct Zn) taken from the Fe Zn binary phase diagram,[36] respectively. Furthermore, the composition of these phases did not change during the simulation. Similarly, the solute concentration in the newly formed $\alpha_\sim$ solid solution close to the tip of the solute rich Γ lamella (c^* 16at. pct Zn) was fixed as constant value determined experimentally.[33] The solute concentration in the α lamella at the α/Γ interface ($c_{\alpha/\Gamma}$) was experimentally established and fixed as constant value (4.11 at. pct Zn) for both the DP and DD reactions simulation.[31,34] In contrast, the zinc concentrations in the α phase lamella ($c(x)$) or in the dissolved phase $\alpha_\sim$ ($c_\sim(x)$) were calculated during DP or DD reaction simulation based on Eqs. [4] and [11], respectively, accordingly to the preliminary conditions for each phase transformation.

To clarify some technical aspects of the modeling and presentation of results, particularly as solute concentration maps, a detailed description of the assumptions implemented in the program with the CA model is provided in this paragraph. Note, that the counters for time, number of CA steps, and movement distance were reset to zero for each discontinuous reaction simulation to make the results easier to interpret. At the beginning of DP reaction simulations, the internal variables with volume fractions of the individual phases at the frontal cells representing the RF state were initialized as 100 pct of a given phase from the nearest Moore neighborhood in which that phase globally had the largest surface contribution. Furthermore, the zinc concentration in the RF cells was determined based on a mass balance. As a result, the zinc concentration in the immobile Γ/α interface was the same as in the α-phase lamella (c_α), while in the cells representing the RF (Γ/α_o, α/α_o, $\Gamma/\alpha_o/\alpha$), the internal variable with zinc concentration takes the value c_o as in the α_o parent phase grain. Since the zinc concentration in the Γ-phase is homogeneous and does not change during the simulation, and is very high (~69 at. pct Zn) relative to the other phases, it was fixed that the Γ-phase lamellae are represented by a single color, maroon, in the 2D maps with solute redistribution. This procedure facilitates the interpretation of the more important results with zinc changes in the α-lamella. Therefore, the zinc concentration in the other phases is presented in a rainbow color scale, with blue representing the lowest Zn concentration and red indicating the highest Zn concentration. Finally, please note that the interfaces between a combination of the following phases α_o, $\alpha_\sim$, $\Gamma_\sim$ are not marked on the DMR images (with black color) because they are also weakly visible in the real microstructures.

IV. RESULTS AND DISCUSSION

Figure 3 shows the results of DP reaction numerical simulation at 723 K (450 °C), for a fixed RF migration velocity, v = 45 nm/s, after 1 seconds of ageing with the Cahn's parameter C equal 7.23. Figures 3(a) and (c) present the successive stages of microstructure evolution in the form of DMR with visible phases and grain boundaries at the beginning (0 seconds) and after 1 seconds, respectively. For the fixed ageing process conditions and assumed steady-state growth, the RF migrated undisturbed at a distance of 45 nm. In the virtual microstructure after the DP reaction, the parent phase α_o, as well as the lamellar structure consisting of Zn-rich Γ phase and Zn-depleted α phase, are present. The corresponding zinc redistribution maps in Figures 3(b) and (d) show the changes in chemical composition of zinc that occurred during the DP reaction. One can observe in Figure 3(d) that the redistribution of Zn concentration across the formed α-lamella is symmetrical because the RF migration velocity was constant as well as the C parameter. The virtual microstructure composed in that way was the input for the CA simulation of the DD reaction.

Figure 4 presents the simulation results of the DD reaction, in the form of DMR images, as an effect of receding RF with constant migration velocity, v = 5 nm/s, after 80 seconds of annealing at a temperature of 923 K (650 °C). In Figures 4(a) and (c) one can

Table II. Data of the z Parameter for One Cycle of Go- and -Stop Motion with Two Extreme C Parameters for λ_α = 150 nm, v_{DD} = 0.5 nm/s and c^* = 16 At. Pct Zn

Stage of Motion/RF Velocity	Time (s)	$z \times 10^7$ (m $^{-1}$)	Cahn's Parameter (–)	
			C_{min} = 1.74	C_{max} = 7.23
Go/v_{DD} = 0.5 nm/s	10	z_1	1.33155	1.63101
	20	z_2	1.35961	1.66619
	30	z_3	1.38723	1.70088
	40	z_4	1.41444	1.7351
	50	z_5	1.44126	1.76887
Stop/v_{DD} = 0 nm/s	60	z_6	1.37678	1.69053
	70	z_7	1.32957	1.63632
	80	z_8	1.24148	1.54061

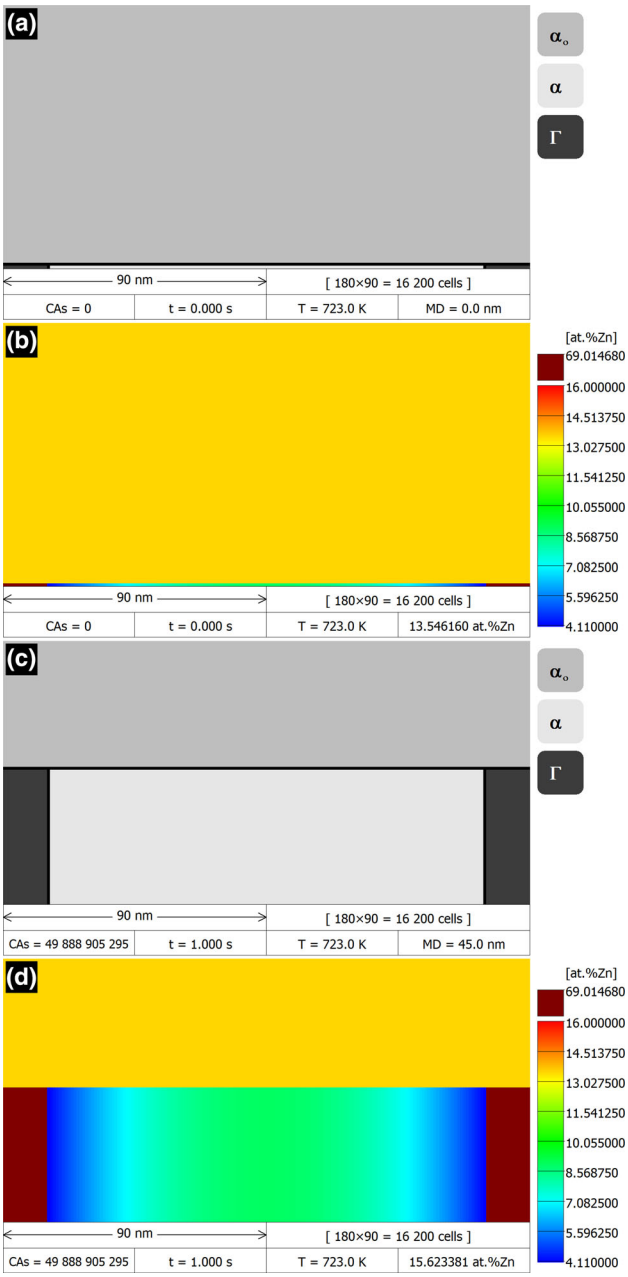

Fig. 3 Simulation results in the form of DMR images (180 × 90 cell CA grid) with visible phases (*a*) and (*c*), and maps with zinc redistribution (*b*) and (*d*), which show the microstructure evolution and chemical composition changes during the DP reaction at 723 K (450°C), for a fixed RF migration velocity, v = 45 nm/s, after 1 s of ageing. (Color version of figure is available online).

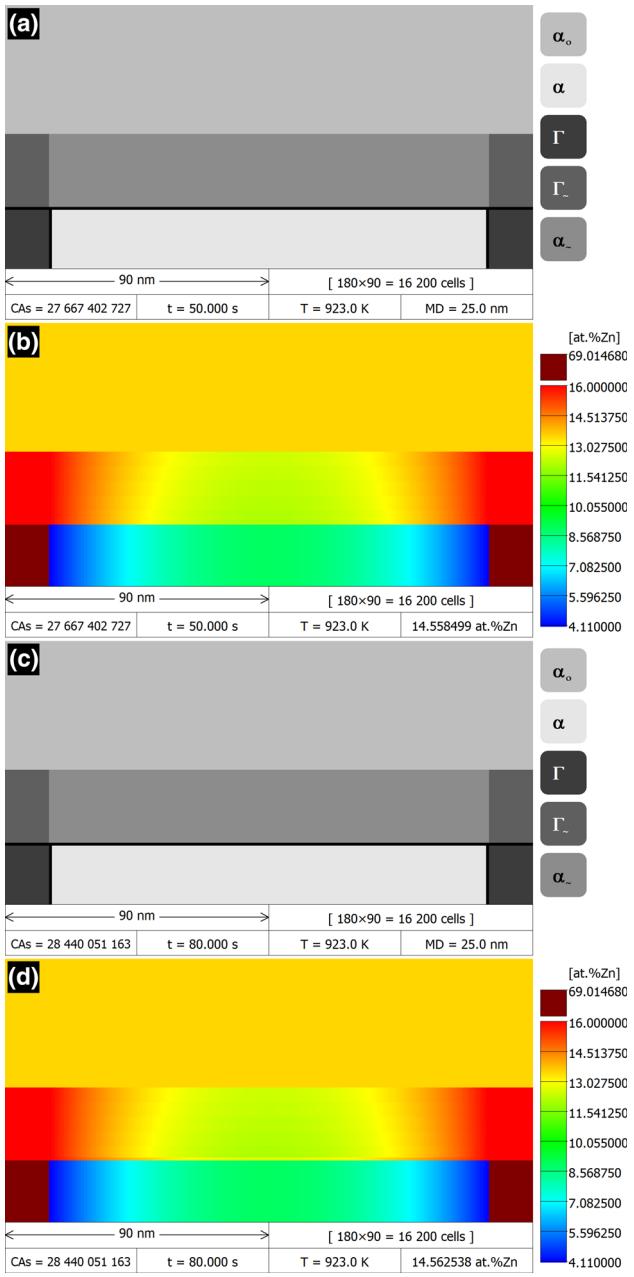

Fig. 4 Simulation results in the form of DMR images (180 × 90 cell CA grid) with visible phases (*a*) and (*c*), and maps with zinc redistribution (*b*) and (*d*), which show the microstructure evolution and chemical composition changes during the DD reaction at 923 K (650 °C), for a fixed RF migration velocity, v = 0.5 nm/s, after 80 s of annealing. (Color version of figure is available online).

observe virtual microstructure evolution at two stages of RF *go-and-stop* motion, *i.e.*, after 50 seconds of movement and 30 seconds of stopped interface, respectively. The RF migrated fluently at a distance of 25 nm after 50 seconds of annealing until the interface was stopped because of not sufficient redistribution of diffusing zinc atoms at the RF. In effect, the driving force of the DD reaction was reduced to zero and in consequence, the RF ceased moving. The virtual microstructure after the DD reaction contains the following phases: resulting dissolved phase $\Gamma_\sim$ and an inhomogeneous $\alpha_\sim$ phase, remaining lamellar structure consisting of Zn-rich Γ phase and Zn-depleted α phase, as well as the untransformed parent phase α_o during DP reaction. Figures 4(b) and (d) depict zinc distribution in all phases present in the structure. In Figure 4(b) one can observe changing redistribution of the Zn concentration in the inhomogeneous $\alpha_\sim$ phase that arises from periodic changes of the z parameter (see Table II). At the beginning of the DD reaction the zinc concentration profile parallel to the RF, with a characteristic "U" shape, features a small gradient. And as the transformation progresses the

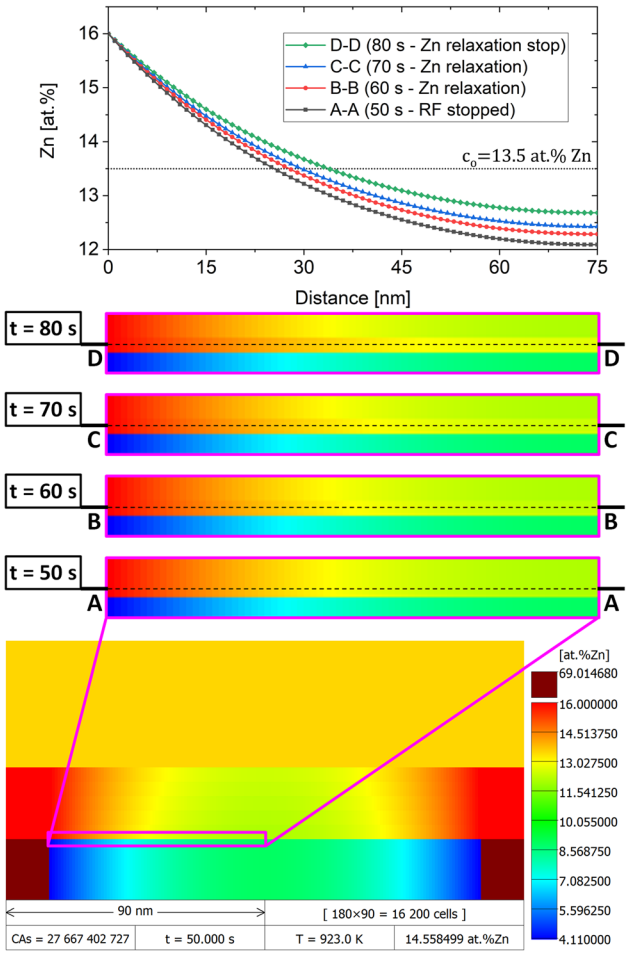

Fig. 5 Simulation results presenting zinc relaxation process at different stages of stopped RF during annealing. (Color version of figure is available online).

gradient of Zn profile becomes bigger which is manifested by gradual increase of the profile "depth" corresponding with increase of the *z* parameter. When the receding RF was stopped during annealing, the solute relaxation process started and the final effect is shown in Figure 4(d). One can observe that the zinc gradient in the RF area has decreased.

A detailed analysis of zinc relaxation is presented in Figure 5, taken from the box assigned on the map with zinc redistribution and depicted in the form of changing Zn profiles at different stages of the stopped RF during annealing. One can interpret the results as follows. At 50 seconds, when the RF stopped, the accumulation of zinc concentration distribution within the RF area was observed, resulting from the supersaturation of Zn during the progression of the DD reaction. After extra 10 seconds (*i.e.*, 60 seconds of the DD reaction simulation), after the initial stage of zinc relaxation at the RF had passed, further reduction in Zn concentration was observed. After 70 seconds, the next relaxation stage occurred, leading to additional changes in the zinc concentration distribution. This process contributes to the equalization of the solute within the RF. After 80 seconds, the solute relaxation stage is finished, and the zinc concentration reached a state which correspond with the beginning of the go- period.

In Figure 6 one can observe a comparison of zinc distribution maps representing an effect of critical values of the *C* parameter on the diffusion kinetics of solute redistribution. The presenting results show that Cahn's parameter *C* strongly influences Zn concentration profiles formed during the DP reaction. Conversely, it has a negligible effect on the zinc distribution during the DD reaction. For a maximum value of $C = 7.23$, a characteristic reverse "U" shape profile of Zn, symmetrical concerning the central axis of the Zn-depleted α lamella, is formed during the DP reaction with a maximum Zn concentration equal to 8.92 at. pct, which is clearly presented on a 3D surface diagram (Figure 6(a)) as well as on a 2D concentration map with a linear analysis (Figure 6(b)) between D D section. Similar analyses were performed for the DP reaction simulation with the parameter $C = 1.74$ (see Figures 6(c) and (d)), which indicates that the maximum concentration of zinc in the α lamella center axis differs significantly from the previous result and equals 5.84 at. pct. On the other hand, the analysis of the DD reaction with zinc distribution shows that the characteristic "U" shape profile of Zn in the inhomogeneous α lamella almost does not change under the influence of the *C* parameter, which is also confirmed in other work.[33] Quantitatively, this is confirmed by the linear analyses of zinc concentrations performed in the α lamella with detected minimum values of Zn concentrations in its axis for individual sections C C and D D (see Figures 6(b) and (d)), which equal 12.44 at. pct Zn, 12.17 at. pct Zn and 12.34 at. pct Zn, 12.02 at. pct Zn for the DD reaction simulations with the $C = 7.23$ and $C = 1.74$, respectively. This effect is also visible on surface diagrams (see Figures 6(a) and (c)) and maps of Zn concentration (see Figures 6(b) and (d)), which exhibit an almost identical gradient intensity of colour. One can conclude that thanks to the presentation of the CA simulation results on the 2D and 3D maps with solute concentration, it is easy to interpret the impact of the kinetic parameters on the zinc distribution during discontinuous reactions.

V. CONCLUSIONS

In this paper, a 2D discrete modeling of two discontinuous reactions, precipitation and dissolution, during ageing and annealing of a Fe-13.5 at. pct Zn alloy, was presented. For this purpose, the cellular automata method coupled with an analytical solution of the mass transport equations (for both DP and DD reactions) has been developed to model the behavior of migrating reaction front along with changes in chemical composition in the lamellar modeling system. The following conclusions from the depicted modeling results can be formulated:

- The developed CA model for discontinuous reactions enables numerical simulation of these phase transformations under conditions defined based on

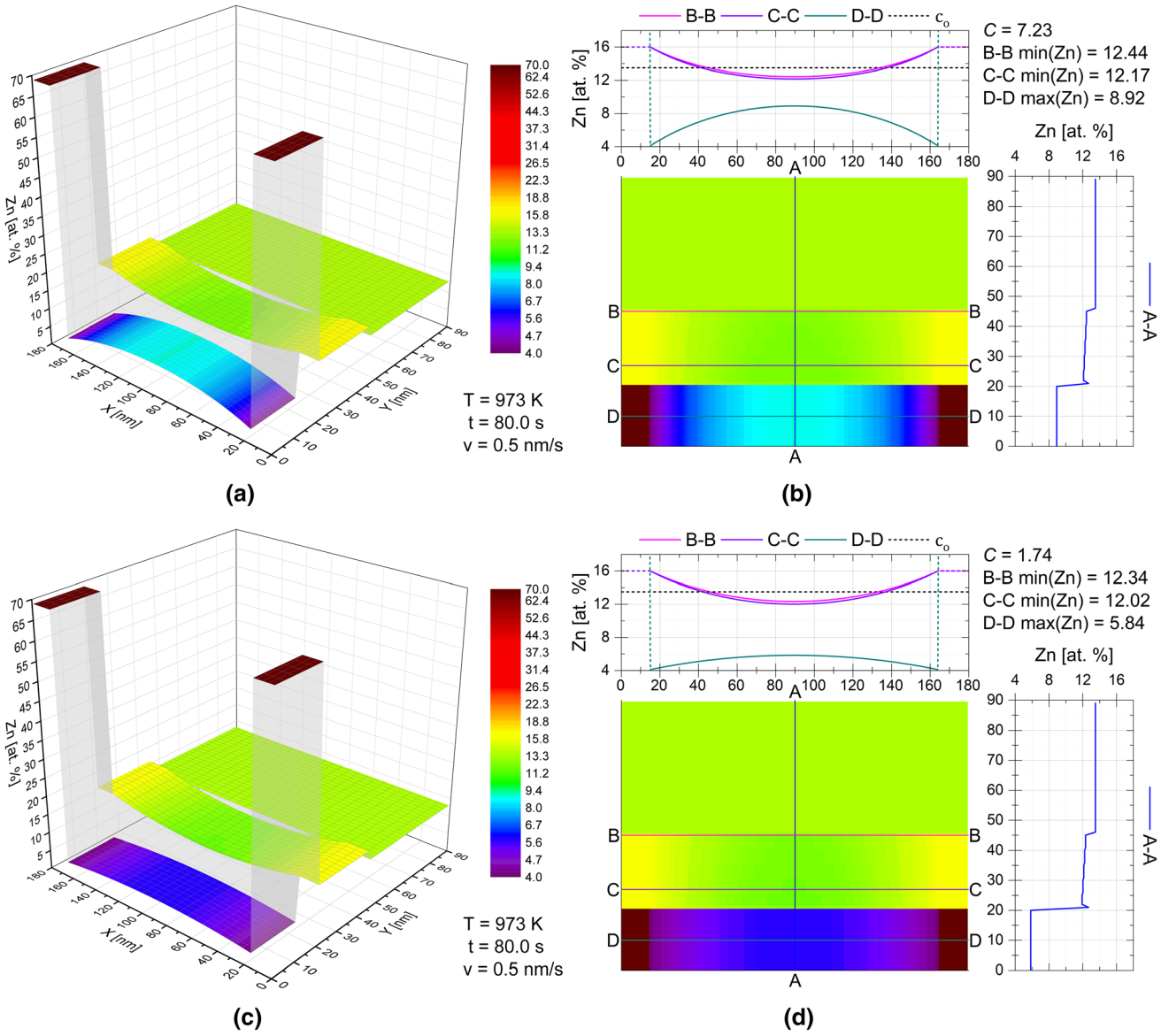

Fig. 6 Comparison of 3D and 2D maps with zinc distribution for two critical values of the C parameter: (*a*) and (*b*) for $C = 7.23$; (*c*) and (*d*) for $C = 1.74$. (Color version of figure is available online).

experimental data and using optimized kinetic parameters (C and z).

- Assuming that the RF is a flat boundary and only the isotropic constant growth at the steady-state is considered, it was possible to simulate microstructure evolution and visualize interface migration during the progress of the DP reaction as well as the receding interphase boundary under the occurrence of the DD reaction using the same lamellar modeling system.
- The CA simulations of discontinuous reactions also allow recording the zinc concentration at the nano-scale level through solute redistribution maps. Consequently, a detailed analysis of the zinc profile change at each stage of RF movement could be performed which has a great significance if they were to be compared with experimental results from analytical electron microscopy investigations.
- The *go-and-stop* motion phenomenon during movement of the RF was simulated using the CA model, which makes it possible to conduct an in-depth analysis of this process in terms of changes in zinc concentration on the phase transformation front.
- The results of CA simulations in the form of 2D and 3D maps of zinc concentration easily allow interpretation of the influence of individual kinetic parameters (C and z) of the DP and DD reactions, respectively, on the formation of zinc concentration profiles due to discontinuous reactions.

Future work should be addressed to direct solving Eq. [2] in the individual CA representing the RF. This would enable simulating the movement of each interface

CA independently at any calculated velocity for a given spacing, boundary geometry, and resulting in different degrees of solute segregation within the limits imposed by local thermodynamic conditions. Such a solution would enhance the comprehensiveness of the analysis of discontinuous reactions and improve the accuracy of numerical simulations of these processes. This, in turn, would enable reliable numerical experiments of ageing and annealing processes.

AUTHOR CONTRIBUTIONS

JO: Conceptualization, methodology, computer implementation, formal analysis, data curation, writing-original draft, visualization; BS: Validation, writing-review and editing; PZ: Conceptualization, resources, supervision, writing-review and editing, project administration, funding acquisition. All authors have read and agreed to the published version of the manuscript.

DATA AVAILABILITY

The data presented in this study are available on request from the corresponding author.

CONFLICT OF INTEREST

On behalf of all authors, the corresponding author states that there is no conflict of interest.

APPENDIX A: THE PROCEDURE TO DETERMINE THE *Z* PARAMETER

The source of data with the z parameter, given in Table II, was obtained using the following algorithm:

(1) Initialization of input parameters for Eq. [4] based on data from Table I, including solute concentration of the matrix (c_o), interfacial solute concentrations ($c_{\alpha/\Gamma}$, c^*), thickness of the α lamella (λ_α), migration velocities of discontinuous reaction fronts (v_{DP} and v_{DD}), and the triple product of diffusivity ($s\delta D_b$).

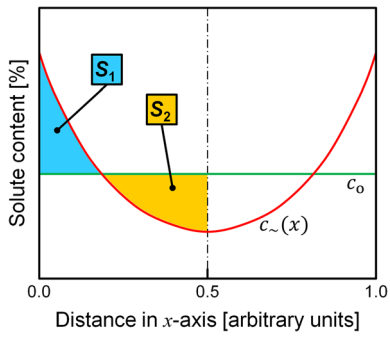

Fig. A1 Schematic representation of solute redistribution following a receding α lamella.

(2) First estimation of the z parameter within an order of magnitude 10^6 10^7 m^{-1}, based on literature data.[33]

(3) Start of the optimization procedure to satisfy the mass concentration balance of the solute (zinc) along the x-axis in the receding α lamella (λ_α).

(4) Calculation of the solute concentration profile ($c_\sim(x)$), with the fixed z parameter based on Eq. [4], that arises in the x-axis in the range of thickness of the receding α lamella (λ_α).

(5) Determination of the areas S_1 and S_2 above and under the level of the initial alloy solute concentration (c_o) for the solute concentration profile, as shown in Figure A1. For this purpose, the trapezoidal rule, a numerical integration method approximating the definite integral of a function, was employed.

(6) Calculation of the new z parameter value using a root-finding algorithm, namely the secant method, where the function f is the difference between areas S_1 and S_2, and the root to be determined is the z parameter. The following equations were used:

$$f \quad S_1(z) \quad S_2(z) \qquad [A1]$$

$$z_n \quad z_{n-1} \quad f(z_{n-1})\frac{z_{n-1} \quad z_{n-2}}{f(z_{n-1}) \quad f(z_{n-2})} \qquad [A2]$$

(7) Calculation of the order of convergence as follows:

$$\varphi \quad |f(z_{n-1}) \quad f(z_{n-2})| \qquad [A3]$$

(8) If the order of convergence is equal to or smaller than the assumed error (1.6×10^{-6}), the procedure is stopped, and the new z parameter is found. If not, repeat steps 4 7.

The algorithm was implemented as a separate computer program using the C++ programming language.

REFERENCES

1. M. Chronowski and P. Zięba: *Arch. Civ. Mech. Eng.*, 2020, vol. 20, p. 35.
2. B.E. Sundquist: *Metall. Trans.*, 1973, vol. 4, pp. 1919 34.
3. M. Hillert: *Metall. Mater. Trans. B*, 1972, vol. 3B, pp. 2729 41.
4. L. Amirouche and M. Plapp: *Acta Mater.*, 2009, vol. 57, pp. 237 47.
5. L. Amirouche and M. Plapp: *Sol. St. Phenom.*, 2011, vol. 172 174, pp. 549 54.
6. P. Zięba: *Arch. Metall. Mater.*, 2017, vol. 62, pp. 955 68.
7. T.C. Duong, R.E. Hackenberg, V. Attari, A. Landa, P.E.A. Turchi, and R. Arróyave: *Comput. Mater. Sci.*, 2020, vol. 175, 109573.
8. A.R. Ladjeroud and L. Amirouche: *Appl. Phys. A*, 2022, vol. 128, p. 582.
9. J. Opara, B. Straumal, and P. Zięba: *Materials*, 2021, vol. 14, p. 4985.
10. J. Zhao, G.-X. Wang, C. Ye, and Y. Dong: *Comput. Mater. Sci.*, 2017, vol. 136, pp. 243 52.
11. G. Shen, C.-W. Zheng, J.-F. Gu, and D.-Z. Li: *Acta Metall. Sin.*, 2018, vol. 31, pp. 713 22.

12. C. Bos, M.G. Mecozzi, and J. Sietsma: *Comput. Mater. Sci.*, 2010, vol. 48, pp. 692 99.
13. C.-W. Zheng and D. Raabe: *Acta Mater.*, 2013, vol. 61, pp. 5504 17.
14. K.J. Song, Y.H. Wei, K. Fang, Z.B. Dong, X.H. Zhan, and W.J. Zheng: *Appl. Math. Model.*, 2015, vol. 39, pp. 5058 72.
15. D. An, S.-I. Baik, S. Pan, M. Zhu, D. Isheim, B.W. Krakauer, and D.N. Seidman: *Metall. Mater. Trans. A*, 2019, vol. 50A, pp. 436 50.
16. J. Opara and R. Kuziak: *J. Met. Mater.*, 2020, vol. 72, pp. 17 31.
17. B. Chopard and M. Droz: *Cellular Automata Modeling of Physical Systems*, Cambridge University Press, Cambridge, 1998, pp. 407 33.
18. S. Wolfram: *A New Kind of Science*. Wolfram Media, 2002, pp. 18 22.
19. D. Raabe: *Adv. Mater.*, 2002, vol. 14, pp. 639 50.
20. K.G.F. Janssens: *Math. Comput. Simul.*, 2010, vol. 80, pp. 1361 81.
21. X. Liu, H. Li, and M. Zhan: *Manuf. Rev.*, 2018, vol. 5, pp. 1 18.
22. M.A. Miodownik: *J. Light Met.*, 2002, vol. 2, pp. 125 35.
23. P. Zięba: *Local Characterization of the Chemistry and Kinetics in Discontinuous Solid State Reactions*, Orekop Ltd., Krakow, 2001, pp. 56 58.
24. L. Madej, L. Rauch, and C. Yang: *Arch. Metall. Mater.*, 2009, vol. 54, pp. 557 65.
25. L. Madej: *Comput. Methods Mater. Sci.*, 2010, vol. 10, pp. 1 13.
26. J. Opara and A. Wrożyna: *Works Inst. Ferr. Metall.*, 2013, vol. 4, pp. 2 7.
27. J.W. Cahn: *Acta Metall.*, 1959, vol. 7, pp. 18 28.
28. J.W. Christian: *Theory of Thermally Activated Growth in the Theory of Transformation in Metals and Alloys*, 1st ed. Pergamon Press, Oxford, 1965, pp. 433 70.
29. K.N. Tu and D.B. Turnbull: *Metall. Trans. A*, 1971, vol. 2, pp. 2509 15.
30. P. Zięba and A. Pawłowski: *Scr. Met.*, 1986, vol. 20, pp. 1653 56.
31. P. Zięba, M. Chronowski, and J. Morgiel: *Arch. Civ. Mech. Eng.*, 2020, vol. 20, p. 76.
32. D.S. Svyetlichnyy: *Comput. Mater. Sci.*, 2010, vol. 50, pp. 92 97.
33. M. Chronowski, J. Opara, B. Straumal, B. Baretzky, and P. Zięba: *Materials*, 2022, vol. 15, p. 3525.
34. P. Zięba, M. Chronowski, J. Opara, O.A. Kogtenkova, and B. Straumal: *Materials*, 2021, vol. 14, p. 1939.
35. M. Chronowski, J. Opara, O.A. Kogtenkova, A.V. Druzhinin, and P. Zięba: *Mater. Lett.*, 2021, vol. 301, 130317.
36. K. Han, I. Ohnuma, K. Okuda, and R. Kainuma: *J. Alloy Compd.*, 2018, vol. 737, pp. 490 504.